JOURNAL OF APPLIED ELECTROCHEMISTRY 9 (1979) 243–253

Investigation of hydrodynamic test systems for the selection of high flow rate resistant materials

E. HEITZ, G. KREYSA, C. LOSS

Dechema-Institut, Theoder-Heuss-Allee 25, D-6000 Frankfurt, Federal Republic of Germany

Received 24 June 1978

Flow-dependent corrosion phenomena can be studied in the laboratory and on a pilot plant scale by a number of methods, of which the rotating disc, the rotating cylinder, the coaxial cylinder and the tubular flow test are the most important. These methods are discussed with regard to mass transfer characteristics and their applicability to flow-dependent corrosion processes and erosion corrosion. To exemplify the application of such methods to materials selection for seawater pumps, corrosion data of non-alloyed and low alloy cast iron are presented.

Nomenclature

(Sh)	Sherwood number
(Re)	Reynolds number
n	exponential of Reynolds number
τ	shear stress (Pa)
η	dynamic viscosity (Pa s)
du/dy	velocity gradient (s^{-1})
ρ	mass density ($kg\,m^{-3}$)
f	friction factor
(Sc)	Schmidt number
i_{cor}, i_c	corrosion current density ($mA\,cm^{-2}$)
i_{lim}	limiting current density ($mA\,cm^{-2}$)
v_{cor}	corrosion rate ($mm\,y^{-1}$ or $g\,m^{-2}d^{-1}$)
u	flow rate ($m\,s^{-1}$)
k	constant
v_{Ph}	phase boundary rate ($g\,m^{-2}d^{-1}$)
z	number of electrons exchanged
F	Faraday number (96 487 $As\,mol^{-1}$)
D	diffusion coefficient (m^2s^{-1})
c	concentration ($kmol\,m^{-3}$)
L	characteristic length (m)
ν	kinematic viscosity (m^2s^{-1})
h	gap width (m)
v	volume rate (m^3s^{-1})
m	rotation rate (min^{-1})
u_{rel}	relative rate of co-axial cylinders ($m\,s^{-1}$)
$\mathfrak{E}_H$	electrode potential versus SHE (V)

1. Introduction

Corrosion phenomena occur on almost all engineering products, equipment and structures, but with increasing size and improved efficiency certain types of corrosion are playing an increasing role. These include the flow-dependent corrosion phenomena of which erosion corrosion is the focus of interest from both a practical and a theoretical point of view. It is the purpose of this paper to compare the mass transfer characteristics of different flow methods by the use of electrochemical limiting current measurements and to evaluate the suitability of the various methods for flow-dependent corrosion testing. From laboratory and pilot scale tests conclusions concerning the kinetics and mechanisms of flow-dependent corrosion processes are drawn. The final aim of such tests is the selection of suitable materials for fluid machinery.

2. Hydrodynamic considerations

Convective mass transport is always influenced by hydrodynamic conditions. In the following sections mass transport is mainly discussed in terms of dimensionless engineering correlations. For a more rigorous treatment the cited literature [1] must be referred to. In connection with

erosion corrosion an interesting parameter should be the shear stress near the corroding wall; therefore the validity of the Chilton–Colburn analogy between mass and momentum transfer is verified for a special system.

2.1. *Hydrodynamically defined test systems*

A number of methods exist for the production of flows in the laboratory and on a pilot scale. These are illustrated diagrammatically in Fig. 1.

Tubular or channel flow is the most widespread method for fluids in chemical engineering. Generally this kind of flow is turbulent. For testing purposes, the tubes form part of a closed loop and the specimens are mounted flush into the wall of a test section [2].

The flow pattern on a rotating disc can be described in terms of physicochemical hydrodynamics. Fig. 1 shows a special kind of rotating disc with a central shaft, which is especially suitable for corrosion tests since it provides surfaces large enough for local corrosion phenomena to be measured [3]. The rotating disc system has the advantage that laminar and turbulent flow can be achieved simply by adjustment of the rotational speed or disc diameter. Suitable design of rotating discs using the principle of enclosed discs leads to very efficient flow systems with high velocity gradients at the specimen surface (circumferential speed up to $100\,m\,s^{-1}$) [4]. Other flow testing systems are free rotating cylinders and coaxial cylinders. Coaxial cylinders are characterized by the circular Couette flow. This system will be used mainly for the evaluation of corrosion resistant materials in this paper.

2.2. *Comparison of mass transfer characteristics*

As usual, mass transfer is characterized by the average limiting current of the reduction of iodine at a platinum surface as a function of a flow quantity such as rotational speed or volume flow rate. The redox system iodine/iodide, already introduced in the 1960s [5], has certain advantages over the mass transfer controlled cathodic reactions such as copper deposition or ferricyanide reduction and is thoroughly described in [6].

For a comparison of the mass transfer it is best to discuss the results in terms of limiting currents as well as in terms of Nusselt's exponential law. As an example, in Fig. 2 the mass transfer characteristics of a circular Couette flow arrangement are given. The experimental set-up has been described earlier [7]. As known from the literature [8] three hydrodynamically distinguished regions are obtained [$(Sh) \sim (Re)^n$]:

(a) laminar region with tangential flow

$$n \leqslant 0{\cdot}60$$

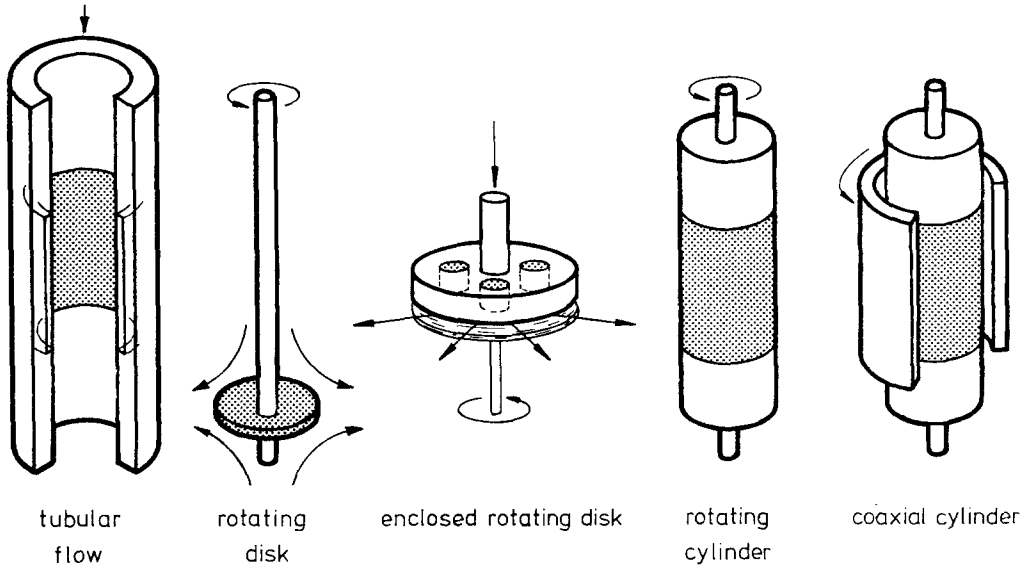

Fig. 1. Various hydrodynamic test systems.

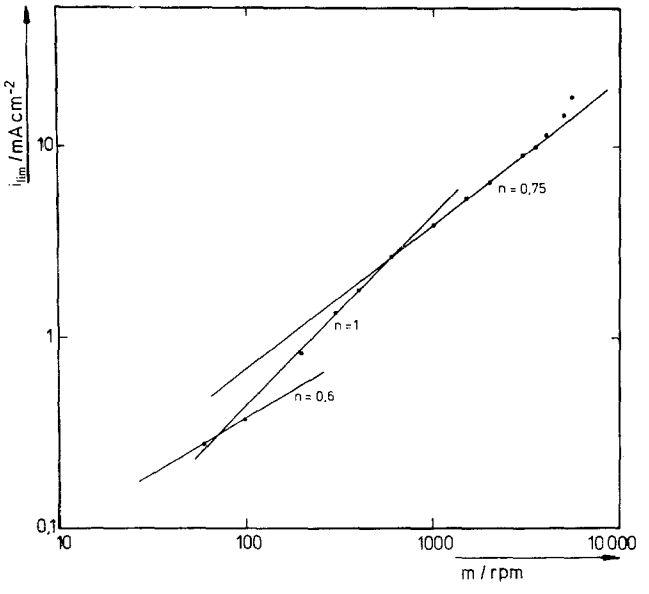

Fig. 2. Mass transfer function for circular Couette flow.

(b) laminar region with Taylor vortices

$$n = 1$$

(c) turbulent region

$$n = 0{\cdot}75$$

It is interesting to note the deviation of the limiting current density at high rotational speeds. This deviation may be due to the fact that, for these conditions, the thickness of the hydrodynamic boundary layer is the same order of magnitude as the surface roughness of the platinum electrode.

Fig. 3 shows the mass transfer to the surface of an enclosed disc. In this case the experimental curve can be approached by tangents with the exponents $n = 0{\cdot}78$ and $n = 0{\cdot}34$.

Mass transfer correlations for various flow models are compared in Table 1, Results correspond to what is to be expected from theory. It is interesting to note that in the laminar region the flow on an enclosed rotating disc resembles a channel flow rather than an open disc flow.

For test purposes it is necessary to choose a suitable flow model. The systems under consideration can be compared on the basis of the mass transfer correlations in Table 1. Correlations of the type shown in Fig. 4 can be obtained by plotting the rotational speed of the rotating cylinder or disc against the tubular flow velocity for equal mass transfer coefficients. Rotational flow systems for the simulation of tubular flow systems can be selected from this kind of diagram. It can be seen

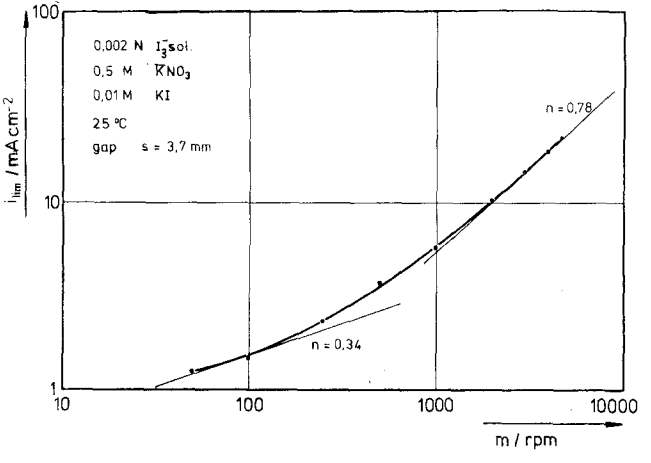

Fig. 3. Mass transfer function for enclosed rotating disc.

Table 1

Mean Sherwood number (Sh)	*Validity range*	*Characteristic length*	*Reference*
A. *Channel flow*			
$2{\cdot}54\ [(Sc)(Re)d_e/L]^{1/3}$	$(Re) < 2300$ (laminar)	hydraulic diameter	[9]
$0{\cdot}023\ (Sc)^{1/3}(Re)^{0{\cdot}8}$	$(Re) > 2300$ (turbulent)		[9]
B. *Rotating disc*			
$0{\cdot}60\ (Sc)^{1/3}(Re)^{1/2}$	$10^2 < (Re) < 10^5$ (laminar)	disc radius	[10]
$0{\cdot}011\ (Sc)^{1/3}(Re)^{0{\cdot}87}$	$(Re) > 10^6$ (turbulent)		[11]
C. *Rotating cylinder*			
$0{\cdot}079\ (Sc)^{0{\cdot}356}(Re)^{0{\cdot}7}$	$10^2 < (Re) < 4 \times 10^5$ (turbulent)	radius	[12]
D. *Coaxial cylinder*			
$2{\cdot}68 \times 10^{-3}\ (Sc)^{1/3}(Re)$	$(Re) < 2{\cdot}74 \times 10^5$	outer radius	this paper
$0{\cdot}0614\ (Sc)^{1/3}(Re)^{0{\cdot}75}$	$2{\cdot}74 \times 10^5 < (he) < 1{\cdot}83 \times 10^6$		this paper
E. *Enclosed rotating disc*			
$17{\cdot}31\ (Sc)^{1/3}(Re)^{0{\cdot}34}$	$9{\cdot}4 \times 10^4 < (Re) < 5{\cdot}95 \times 10^5$ $h = 0{\cdot}37$ cm $v = 2{\cdot}5\ m^3h^{-1}$	disc radius	this paper
$0{\cdot}0498\ (Sc)^{1/3}(Re)^{0{\cdot}78}$	$(Re) > 5{\cdot}95 \times 10^5$		this paper

that in the turbulent flow region the rotating disc, rotating cylinder and cylinder Couette flow with equal diameter and rotational velocity correspond to the same tubular flow. The same holds for the free rotating and enclosed rotating discs. However, in the laminar region the enclosed disc provides much higher mass transfer coefficients than the free rotating disc and therefore corresponds to a tubular velocity ten times as great.

2.3. *Chilton–Colburn analogy for estimating the shear stress*

The shear stress of a flowing liquid on the surface of a corroding metal is important with regard to the stability of its surface layers. In some mechanisms of erosion corrosion it is assumed that the shear stress destroys the surface layers that slow down corrosion processes.

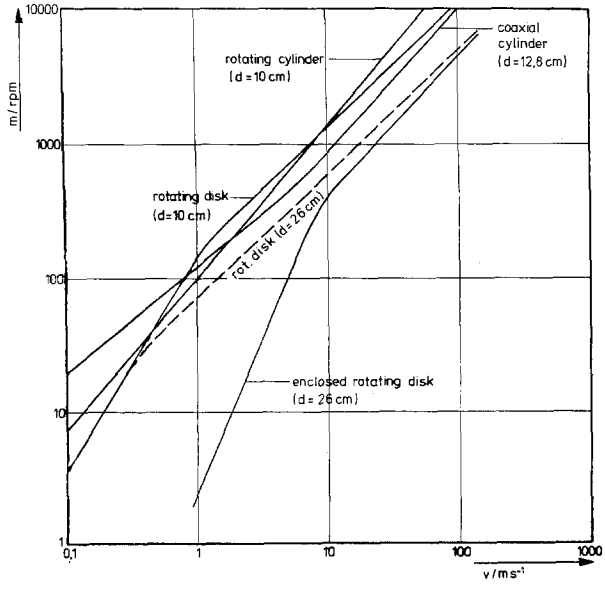

Fig. 4. Correlation between rotational speed and tubular flow velocity at equal mass transfer coefficients.

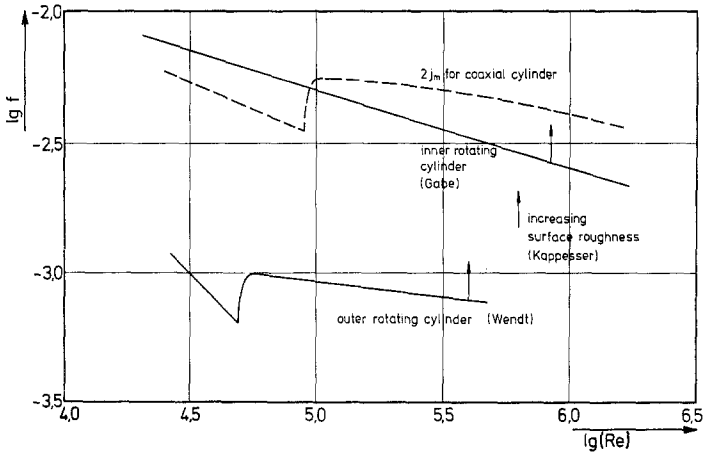

Fig. 5. Verification of Chilton–Colburn analogy. Dashed curve: own measurements.

The Chilton–Colburn analogy is derived as follows:

$$\text{shear stress} \quad \tau = \eta \frac{\mathrm{d}u}{\mathrm{d}y} \quad \text{(Newton's law)}.$$

Shear stress and flow velocity are correlated by the Fanning friction factor f

$$\tau = f(\rho/2)u^2.$$

The Chilton–Colburn analogy between mass and momentum transfer is given by

$$j_m = f/2$$

with

$$j_m = \frac{(Sh)}{(Re)(Sc)^{1/3}}.$$

Fig. 5 shows the dependence of the friction factor on the Reynolds number for coaxial cylinders with inner [12] or outer [13] rotating cylinders. The dashed curve is the relationship between the friction factor and the Reynolds number with friction factors obtained from experimental results by use of the Chilton–Colburn analogy. Since a coaxial cylinder with a rotating outer cylinder but with the specimen mounted at the inner cylinder was used in the experimental arrangement, the curve corresponds to the mass transfer to a rotating outer cylinder with its typical transition from laminar to turbulent flow (Taylor vortices). However, the values of the friction factor are in the range of those obtained on the rotating inner cylinder. If, in addition, the surface roughness which gives rise to an increase of the friction factor is taken into account [14], it may safely be assumed that the Chilton–Colburn analogy is valid and therefore shear stress data may be estimated from mass transfer measurements. On the other hand there is a lack of information about the mechanical properties of the surface film. Nevertheless, the magnitude of the shear stresses at the specimen surface is very small so that observed erosion corrosion in the absence of abrasive particles cannot be explained on the basis of a simple mechanical model [7, 15, 16].

3. Application to flow-dependent corrosion processes

3.1. *Influence of flow rate, time, oxidant concentration and potential*

Experiments in a rotating coaxial cylinder apparatus [11, 12] with a number of corrosion systems with practical relevance normally revealed correlations between corrosion currents (from polarization resistance) and rotational speed of the kind shown in Fig. 6. After a region in which the mixed kinetics of mass transfer and phase boundary reaction predominate (region I), a region virtually independent of flow rate follows (region II) and finally the typical erosion corrosion appears, characterized by an increase in the corrosion rate (region III). It is important to note that this region of erosion corrosion only develops after an induction time of several hours.

The discussion of region I may be based on a two-step corrosion mechanism, with oxygen diffusing to the metal surface and reacting in the cathodic partial step. This is well illustrated by the flow-dependent corrosion of non-alloyed steel in seawater (Fig. 7).

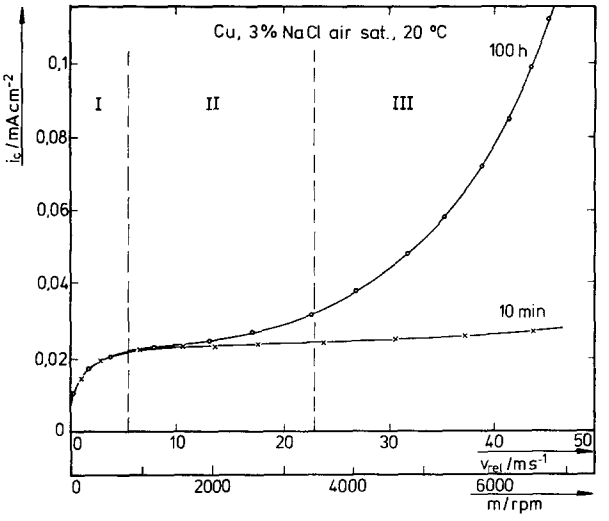

Fig. 6. Dependence of corrosion rate on flow velocity.

After an initially strong flow dependence the corrosion rates decrease and finally become independent of flow, due to the growth of a surface layer. These experiments were carried out with the specimen inserted into the wall of a flow channel used for simulation of the conditions of thermal seawater desalination [2].

If the results shown in Fig. 6 (coaxial system) are transferred to the usual log i versus log (Re) plot the curves in Fig. 8 are obtained.

No simple mass transfer relationship exists and no transition from laminar to turbulent flow can be seen. Another mechanism must therefore be assumed, at least in the erosion corrosion region. Similar results have been obtained by another author, but using a rotating disc [17].

A useful method for investigating the mechanism in greater detail is to take current–potential curves of specimens attacked by erosion corrosion and of specimens in the initial stage with the flow rate taken as a parameter. In Fig. 9 erosion corroded samples show a definite mass transfer dependence of the cathodic partial step. In Fig. 10, which gives the behaviour of non erosion corroded samples, the anodic partial step is mass transfer dependent. In this connection the difference in the flow models is of no relevance since no quantitative kinetic data are evaluated.

The change in the rate-determining step from the anodic to the cathodic side during the appearance of erosion corrosion is due to the fact that the existence of a plain metal surface speeds up the anodic processes (including mass transfer). At the same time, the cathodic partial reaction is shifted towards the limiting current region.

By calculating the bulk limiting diffusion currents of the oxygen for the various regions in Fig. 6 (co-axial system) and plotting these as the percentage ratio i_{cor}/i_{lim} versus rotational speed, the curves in Fig. 11 are obtained. Over the whole measured range, the corrosion current only amounts to a small proportion of the limiting oxygen diffusion current, suggesting that pore diffusion is the controlling factor.

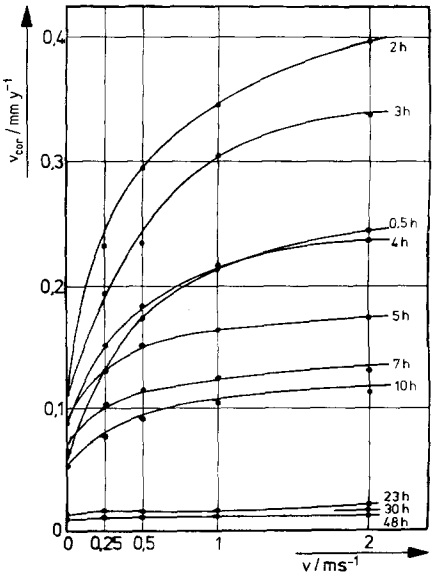

Fig. 7. Dependence of corrosion rate on flow velocity and time; non-alloyed steel in seawater; 110° C; 2 ppb oxygen.

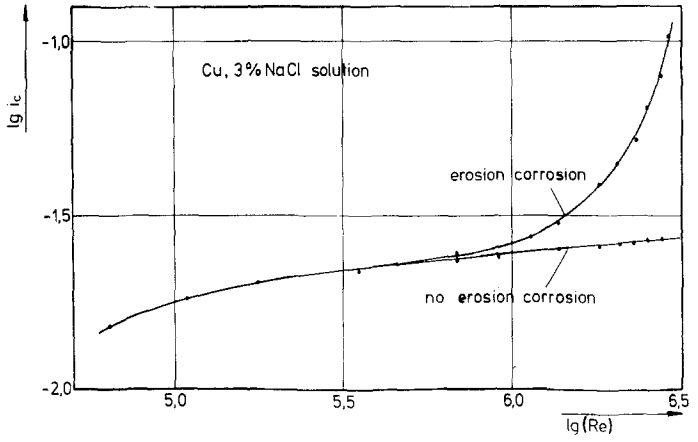

Fig. 8. Dependence of corrosion rate on Reynolds number.

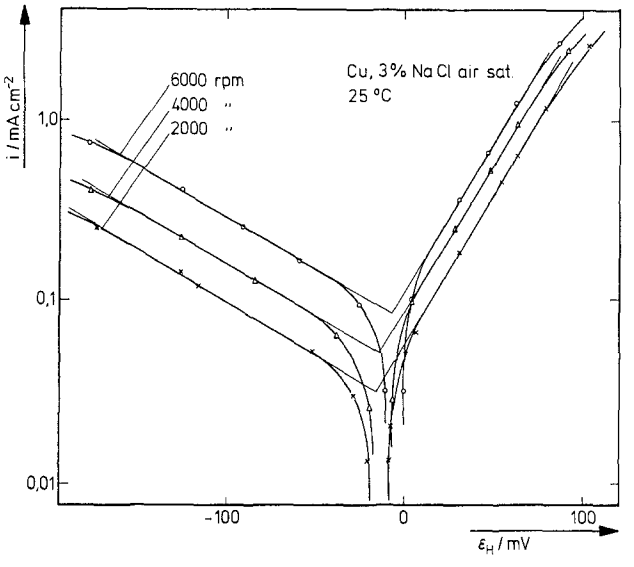

Fig. 9. Tafel plots for erosion corroded samples (coaxial cylinder).

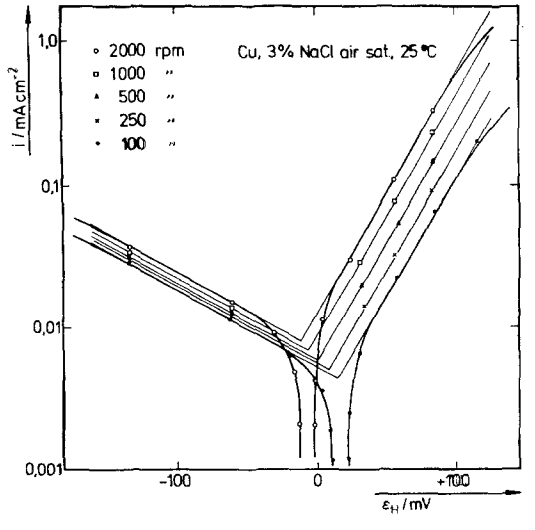

Fig. 10. Tafel plots for non erosion corroded samples (rotating disc).

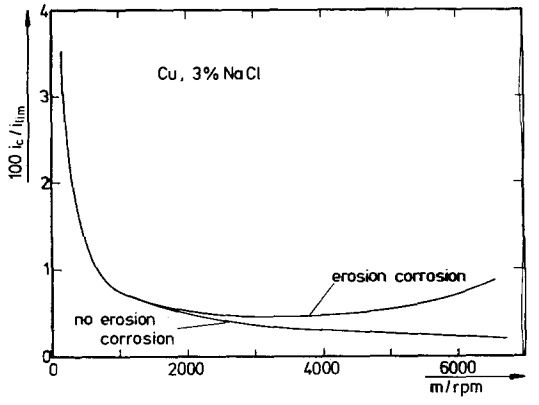

Fig. 11. Rotation dependence of corrosion current density related to oxygen diffusion limiting current density.

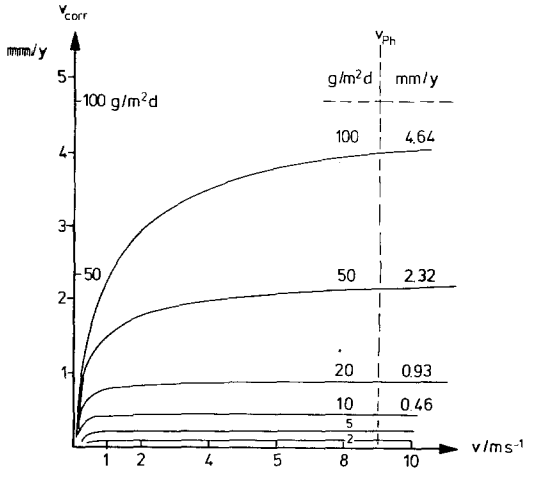

Fig. 12. Flow dependence of corrosion rate (calculated for iron in aerated water).

It is possible to calculate the relationship between phase boundary reaction rates and flow rates on the basis of the consecutive two-step mechanism mentioned above. Assuming the occurrence of a corrosion process by neutral aerated water on the inner side of a steel tube, the overall corrosion rate is a function of the hydrodynamic conditions and the reaction rate at the phase boundary. For first-order reactions with steady-state conditions the following general equation can be given [7]:

$$v_{corr} = \frac{1}{(1/ku^{0.8}) + (1/v_{Ph})}.$$

This equation contains the flow rate controlled mass transfer rate $ku^{0.8}$ and the phase boundary rate v_{Ph}. The constant k can be calculated from the corresponding Sherwood number in Table 1 and the correlation between limiting current density i_{lim} and Sherwood number (Sh) [6]:

$$i_{lim} = (Sh)\frac{zFDc}{L}$$

with z = 4 (for oxygen)
F = 96 487 As mol^{-1}
D = $1{\cdot}9 \times 10^{-5}$ cm^2 s^{-1} (oxygen diffusion coefficient)
c = $0{\cdot}25 \times 10^{-6}$ mol cm^{-3} (oxygen concentration)
L = 5 cm (tube diameter)
ν = 0·01 cm^2 s^{-1} (kinematic viscosity)
u = flow rate in cm s^{-1}.

If all rates are expressed in g m^{-2} d^{-1} the following equation is obtained:

$$v_{corr} = \frac{1}{(1/2{\cdot}46u^{0.8}) + (1/v_{Ph})}$$

which gives the set of curves shown in Fig. 12, for different phase boundary rates.

From these curves and for the given corrosion system the following conclusions can be drawn:

(a) for small phase boundary rates the overall corrosion is not flow dependent ($v_{Ph} < 5$ g m^{-2} d^{-1});

(b) for high phase boundary rates ($v_{Ph} > 50$ g m^{-2} d^{-1}) the overall corrosion rate is flow dependent up to 10 m s^{-1} for a 5 cm diameter tube;

(c) for medium phase boundary rates (e.g. $v_{Ph} = 20$ g m^{-2} d^{-1}) there exists a flow-dependent region up to approximately 2 m s^{-1}.

The calculated curves allow for an estimation of the flow dependencies of the system iron/aerated water if only one corrosion rate at one flow velocity is known. If, for example, an active iron surface corrodes at 0·5 m s^{-1} with a rate of 35 g m^{-2} d^{-1}, an increase in flow velocity to 3 m s^{-1} will double the corrosion rate. If the corrosion rate is already as low as 5 g m^{-2} d^{-1} an increase in flow velocity will not change the overall corrosion rate. In this case the phase boundary reaction is rate determining, for example as a consequence of an oxide layer on the iron surface. However, all these considerations only hold for as long as the mechanism assumed (uniform corrosion and absence of erosion corrosion) does not change.

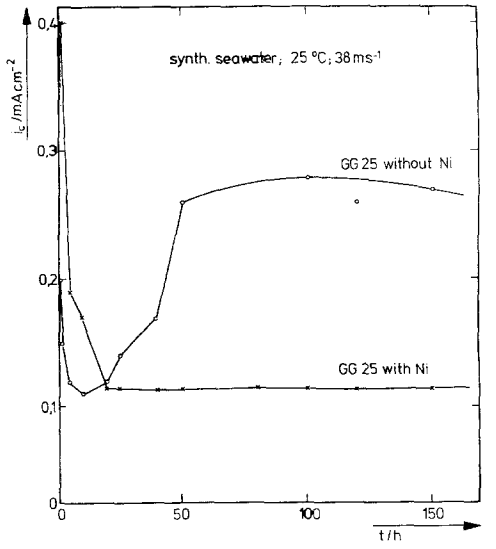

Fig. 13. Time dependence of corrosion rate; alloyed and non-alloyed cast iron in synthetic seawater; 25° C; 38 m s^{-1}; pH = 8.

3.2. *Materials selection for seawater pumps*

The rotating coaxial cylinder apparatus was used for the selection of corrosion resistant materials for the casings of seawater pumps. Two materials had to be taken into consideration: plain cast iron and cast iron alloyed with nickel (composition: 3·25 wt% C, 2·34 wt% Si, 0·61 wt% Mn, 0·14 wt% P, 0·1 wt% S, traces of Ni or 2·5 wt% Ni). The solution was synthetic seawater (ASTM). Specimens were mounted flush into the inner cylinder of the test apparatus and runs were started at a rotational speed of almost 6000 rev min^{-1} (circumferential speed: 38 m s^{-1}). The corrosion rates were measured electrochemically by means of polarization resistance measurements, which in this case gave results equal to weight loss measurements. The results are given in Fig. 13. They may be summarized as follows:

(a) high initial corrosion rates, due to the mechanically treated metal surface, decrease after a few hours;

(b) Ni alloyed cast iron reaches a steady state;

(c) non-alloyed cast iron gives a corrosion rate minimum after approximately 10 h test time and reaches a much higher steady-state level.

From these results it can be concluded that erosion corrosion of non-alloyed cast iron has a characteristic induction time which, in the case given above, amounts to 20 h. Therefore, tests for sufficient duration have to be carried out, as scaling-up in time is not possible. On the other hand, if the cast iron contains nickel, the corrosion is uniform within the velocity range tested and a steady state is reached, and thus scaling-up in time is possible.

Some insight into the difference between non-alloyed and low-alloyed cast iron is given by photographs of the specimen surface after the tests (Figs. 14 and 15). Whereas the non-alloyed material shows a coarse surface layer, the alloyed material has a finer surface. It is assumed that in the latter case the Ni produces a mechanically more stable surface layer. The stability may be due to a finer distribution of the graphite in the metal matrix of the Ni-alloyed cast iron.

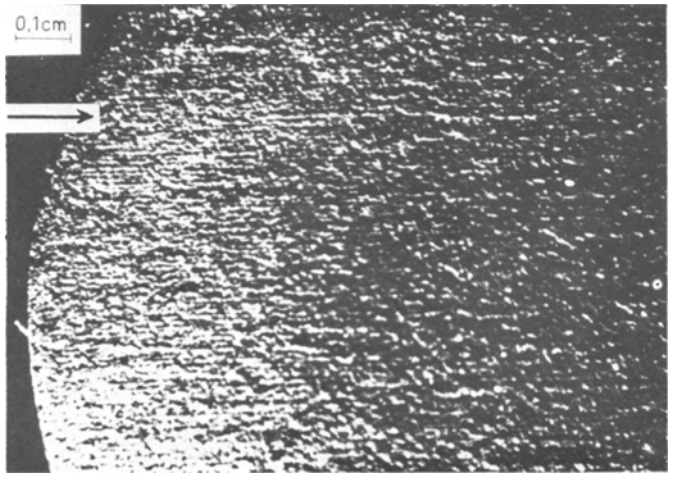

Fig. 14. Photograph of sample surface after corrosion test; cast iron; 38 m s^{-1}; → flow direction.

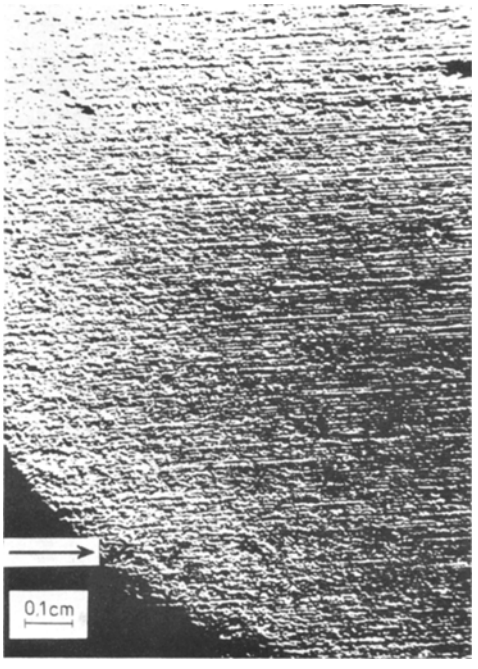

Fig. 15. Photograph of sample surface after corrosion test; Ni alloyed cast iron; 38 m s^{-1}; → flow direction.

4. Conclusions

(a) A number of methods exist for testing flow-dependent corrosion processes. For the laboratory tests the rotating disc is the most suitable, whereas for pilot tests the rotating coaxial cylinder, the enclosed rotating disc and tubular or channel flow can be successfully applied.

(b) It is possible to correlate the rotational speed of circular systems with tubular or channel flow velocities by measuring the limiting current. In the turbulent region all rotational systems of approximately equal geometrical dimensions have an equal mass transfer characteristic. In the laminar flow regime the enclosed rotating disc is considerably better than the other rotational systems.

(c) According to proposed mechanisms, erosion corrosion is caused by the destruction of surface layers as a consequence of shear stress of a flowing liquid. It is shown that the shear stress can be correlated with the mass transfer coefficient (Chilton–Colburn analogy). However, critical flow velocities for given corrosion systems cannot be given, since the mechanical properties of the protective layers are not known.

(d) Investigations into the flow dependence of various corrosion systems give results which can be explained on the basis of combined mass transfer and phase boundary reactions or with pore diffusion as the controlling factor.

(e) When selecting a suitable material for pump casings in seawater under given flow conditions, it is necessary to choose a Ni alloyed cast iron. If only non-alloyed material is available the flow velocity in the pump has to be lowered (with a consequent decrease in power). This would suggest that further experiments at lower flow velocities should be carried out. On the basis of such experiments a cost minimum could be evaluated by an optimization calculation. The material would form part of the investment costs, the flow velocity being related to the running costs.

Acknowledgements

Part of this work was carried out with the financial support of the Bundesinnenministerium and Bundesministerium für Forschung und Technologie within the framework of the following projects: Korrosion; COST 53; Forschungs- und Entwicklungsprogramm 'Korrosion und Korrosionsschutz'.

The authors are indebted to K. Heil, H. Hofmann and R. Manner for carrying out part of the experimental work.

References

[1] D. J. Pickett, 'Electrochemical Reactor Design', Elsevier, Amsterdam (1977).
[2] R. Manner and E. Heitz, *Werkst. u. Korr.* **29** (1978) 559.
[3] F. Franz, E. Heitz, G. Herbsleb and W. Schwenk, *ibid* **24** (1973) 97.
[4] G. C. Pini, E. Bachmann and G. Orkenyi, *Werkst. u. Korr.* **27** (1976) 693.
[5] A. C. Riddiford in 'Advances in Electrochemistry and Electrochemical Engineering' (edited by P. Delahay), Vol. 4 (1966) p. 47.
[6] E. Heitz and G. Kreysa, 'Grundlagen der Technischen Elektrochemie', Verlag Chemie, Weinheim (1977).
[7] C. Loss and E. Heitz, *Werkst. u. Korr.* **24** (1973) 38.
[8] J. S. Newman, 'Electrochemical Systems', Prentice-Hall, Englewood Cliffs (1973).
[9] D. J. Pickett, *Electrocheim. Acta* **19** (1974) 875.
[10] B. G. Levich, 'Physicochemical Hydrodynamics', Prentice-Hall, Englewood Cliffs (1962).
[11] O. Dossenbach, *Ber. Bunsenges. phys. Chem.* **80** (1976) 341.
[12] D. R. Gabe, *J. Appl. Electrochem.* **4** (1974) 91.

[13] F. Wendt, *Ing.-Archiv* **4** (1932) 577.
[14] R. Kappesser, O. Cornet and R. Greif, *J. Electrochem. Soc.* **118** (1971) 1957.
[15] E. Heitz and C. Loss, *Proceedings 5th International Congress Metal Corrosion*, NACE, (1974) 477.
[16] B. C. Syrett, *Corrosion NACE* **32** (1976) 242.
[17] R. Bartonicek, *Werkst. u. Korr.* **28** (1977) 232.